Elastic Properties and Elastic Anisotropy of ZrN_2 and HfN_2

Jianguo Zhang[a,*], Ruijiao Jiang[a], Yangyang Tuo[a], Taian Yao[a] and Dongyun Zhang[b]
[a]School of Sciences, Xi'an University of Architecture and Technology, Xi'an 710043, China
[b]National Supercomputing Center in Shenzhen, Shenzhen 518055, China

(Received August 3, 2018; in final form October 13, 2018)

In this paper, first-principle calculations were used to determine the mechanical and electronic properties as well as the elastic anisotropy of ZrN_2 and HfN_2. Young's modulus, shear modulus, Poisson's ratio, and anisotropy under different pressures were studied. It has been shown that ZrN_2 and HfN_2 can be stable up to at least 100 GPa. The value of B/G increased with pressure, indicating that both ZrN_2 and HfN_2 are ductile. The values of A^U, A_1, and A_2 are not 0, signifying that both ZrN_2 and HfN_2 have anisotropy.

DOI: 10.12693/APhysPolA.135.546

PACS/topics: elastic properties, first-principle calculations, nitrides, elastic anisotropy

1. Introduction

The rapid development of modern science and technology has put forward more and more rigorous requirements on the properties of materials. Hardness is one of the most important and basic index in many of the properties of materials. Superhard materials usually have large strength, high hardness, great brittleness, etc. Alloying elements, containing multi-component and higher activities, such as Ni, Cr, V, Mo, Co, Al, Ti, or compound materials, containing metal and nonmetals, are called superhard materials [1]. The study on the synthesis and properties of superhard materials have been one of the key focus of material science research.

Transition metal nitrides have excellent properties such as good mechanical, optical, and magnetic properties. Owing to these excellent properties they are used as corrosion resistant materials, optical coating materials, as well as electrode materials in optoelectronic industry. In addition to this, they stimulated interest in basic research and application. Colmenares et al. [2] theoretically made an analysis on RuN_2. Then, Yu et al. [3–6] conducted a theoretical study and analysis on PtN_2, OsN_2, IrN_2, RuN_2, and RhN_2. WC_X, ZrN_X, TiN_X, and VC_X are commonly used in hard coating, but they do not meet the requirements of all of the protective layers [7]. The most critical factor is the high hardness at high temperatures. Recently, researchers have payed more attention to the study of transition metal nitrides such as PtN_2, IrN_2, RuN_2, and OsN_2. They have very high bulk modulus [8–12], and these inherent advantages make the above compounds worth studying. Soto et al. conducted an analysis of the equivalent structure and composition of novel transition metal nitrides and early transition metal nitrides, and revealed their stability and the relative bond length. They performed self-consistent calculations, using MeN_2 compound using several structural changes and thereby Me can be substituted with Hf, Ta, Re, or Os [13].

In this study, the structural characteristics and elastic properties of ZrN_2 and HfN_2, under pressures from 0 to 100 GPa, were examined, and using the outcome, the elastic anisotropy was also analyzed in detail.

2. Theoretical method

First principle calculations using plane-wave pseudopotential method based on density functional theory (DFT) [14, 15] utilizing the software CASTEP [16] were attempted. In the calculation, the Ceperley–Alder–Perdew–Zunger (CA-PZ) method of the local density approximate (LDA) [17, 18] was used for the exchange correlation of electrons. The interaction between ionic and valence electrons is ultrasoft pseudopotential; the plane wave cutoff energy is 340 eV; k-point grid is taken as $6\times6\times5$. The total energy convergence tests showed that convergence to within 0.001 eV/atom was accomplished with the above mentioned calculation parameters.

3. Results and discussion

3.1. Structural properties

The crystal structures of ZrN_2 and HfN_2 are shown in Fig. 1a and b, respectively. The space group of ZrN_2 and HfN_2 are $I4/mcm$. The calculated lattice parameters of ZrN_2 and HfN_2 are shown in Table I, and for comparison the previous results are also listed. a_0, c_0, and V_0 are the equilibrium structural parameters at 0 GPa and 0 K. Obviously, our results are in good agreement with the previously reported values. Moreover, the pressure dependence of normalized parameters a/a_0, c/c_0 and V/V_0, as a function of pressure for ZrN_2 and HfN_2, are shown in Fig. 2. For ZrN_2, the relationships between a/a_0, c/c_0, and pressure are

$$\frac{a}{a_0} = 0.999 - 9.650\times10^{-4}P + 2.993\times10^{-6}P^2, \quad (1)$$

*corresponding author; e-mail: 1247224860@qq.com

$$\frac{c}{c_0} = 0.999 - 1.010 \times 10^{-3} P + 2.881 \times 10^{-6} P^2, \quad (2)$$

whereas, for HfN_2, they are

$$\frac{a}{a_0} = 0.999 - 8.901 \times 10^{-4} P + 2.709 \times 10^{-6} P^2, \quad (3)$$

$$\frac{c}{c_0} = 0.999 - 8.882 \times 10^{-4} P + 2.786 \times 10^{-6} P^2. \quad (4)$$

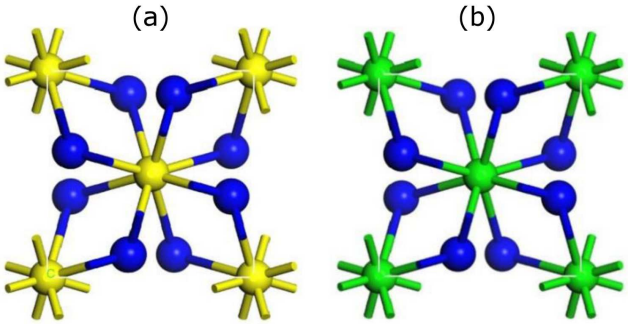

Fig. 1. (a) Crystal structure of ZrN_2. The yellow and blue spheres represent Zr and N atoms. (b) Crystal structure of HfN_2. The green and blue spheres represent Hf and N atoms.

TABLE I

Calculated crystal lattices [Å], unit cell volume [Å^3] for ZrN_2 and HfN_2.

Crystal	Source	a_0	c_0	V_0
ZrN_2	this work	4.522	5.669	115.949
	exp. [19]	4.596	5.767	121.793
HfN_2	this work	4.561	5.721	118.995
	exp. [19]	4.555	5.683	117.854

As the pressure increases, the ratio of the volume of primitive cell ranges from 1.0 to 0.804, and the ratios of the lattice constants a/a_0, c/c_0 decrease with pressure. It is clear that c/c_0 decreases more rapidly than a/a_0 with an increase in pressure for ZrN_2 (Fig. 2a). It is shown that ZrN_2 is more easily compressed along c-axis of the crystal than along a-axis. As the pressure increases, the ratio of the volume of primitive cell is from 1.0 to 0.823, and the ratios of the lattice constants a/a_0, c/c_0 decrease with pressure. It is clear that a/a_0 decreases more rapidly than c/c_0 with an increase in pressure for HfN_2 (Fig. 2b). It is shown that HfN_2 is more easily compressed along a-axis of the crystal than along c-axis.

3.2. Elastic properties

For a crystal, there are twenty-one independent elastic constants. According to the symmetry of crystal, the number of independent elastic constants can be reduced. ZrN_2 and HfN_2 are of tetragonal symmetry, and thus have six independent elastic constants and the elastic stiffness tensor matrix can be expressed in the following way [19]:

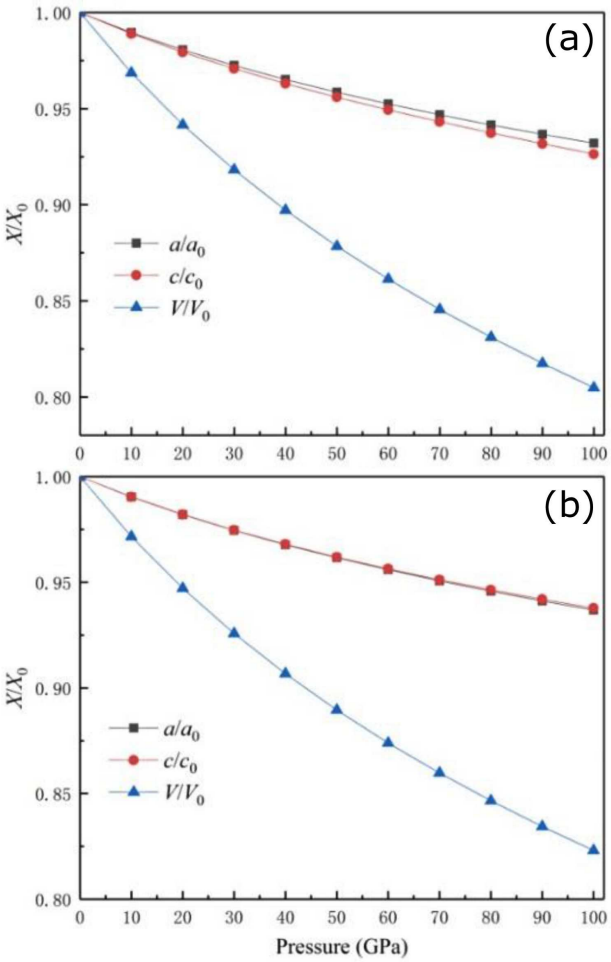

Fig. 2. (a) The calculated normalized volumes and lattice parameter as a function of pressure for ZrN_2. (b) The calculated normalized volumes and lattice parameter as a function of pressure for HfN_2.

$$C = \begin{bmatrix} C_{11} & C_{12} & C_{13} & 0 & 0 & 0 \\ & C_{11} & C_{13} & 0 & 0 & 0 \\ & & C_{33} & C_{44} & 0 & 0 \\ & & & C_{44} & 0 & 0 \\ & & & & C_{44} & 0 \\ & & & & & C_{66} \end{bmatrix}. \quad (5)$$

Calculated elastic constants C_{ij}, bulk modulus B, shear modulus G, Young's modulus E, Poisson's ratio ν, calculated by the Voigt–Reuss–Hill approximations [20], and B/G ratio of ZrN_2 and HfN_2 are shown in Tables II and III, respectively. Their existence conditions of the stability are shown as follows:

$$C_{44} > 0, \quad (6)$$

$$C_{11} > |C_{12}|, \quad (7)$$

$$(C_{11} + C_{12}) C_{33} > 2C_{13}^2. \quad (8)$$

The mechanical stability of crystal under isotropic pressure is expressed as follows [21]:

$$\hat{G} = \begin{bmatrix} \tilde{C}_{11} & \tilde{C}_{12} & \tilde{C}_{13} & 0 & 0 & 0 \\ & \tilde{C}_{22} & \tilde{C}_{23} & 0 & 0 & 0 \\ & & \tilde{C}_{33} & 0 & 0 & 0 \\ & & & 4\tilde{C}_{44} & 0 & 0 \\ & & & & 4\tilde{C}_{55} & 0 \\ & & & & & 4\tilde{C}_{66} \end{bmatrix}. \quad (9)$$

Here,

$$\tilde{C}_{\alpha\alpha} = C_{\alpha\alpha} - P, \quad \alpha = 1, 2, \ldots, 6, \quad (10)$$

$$\tilde{C}_{12} = C_{12} + P, \quad (11)$$

$$\tilde{C}_{13} = C_{13} + P. \quad (12)$$

For tetragonal crystals, the mechanical stability of the crystal occurs under the following conditions:

$$\tilde{C}_{44} > 0, \quad (13)$$

$$\tilde{C}_{11} > \left|\tilde{C}_{12}\right|, \quad (14)$$

$$\tilde{C}_{11} + 2\tilde{C}_{12} > 0. \quad (15)$$

The results indicated that ZrN_2 and HfN_2 are stable from 0 GPa to 100 GPa.

The bulk modulus B and shear modulus$G$ determine the resistance to plastic deformation and crack propagation of materials. Pugh [22] showed that an indication of the ductile or brittle characteristics can be estimated by the ratio of B/G. With an increase in pressure, it could be seen that B and G of ZrN_2 as well as HfN_2 showed a monotonic growth as indicated in Tables II and III, respectively. If $B/G > 1.75$, the material is defined to be ductile, otherwise it is brittle. For ZrN_2 and HfN_2, the ratio of B/G at 0 GPa is 1.719 and 1.550 respectively, which indicates that they are one type of brittle material. When the pressure increases from 0 GPa to 100 GPa, the value of B/G of ZrN_2 increases from 1.719 to 3.102, whereas, for HfN_2, it increases from 1.550 to 2.168. It is shown that the value of B/G increases with an increase in pressure, and ZrN_2 and HfN_2 exhibit more excellent toughness under stress.

TABLE II

Calculated elastic C_{ij} [GPa], bulk modulus B [GPa], shear modulus G [GPa], Young's modulus E [GPa], Poisson's ratio ν, and B/G ratio of ZrN_2 under pressure [GPa].

P	C_{11}	C_{33}	C_{44}	C_{66}	C_{12}	C_{13}	B	G	E	B/G	ν
0	482	653	132	301	299	102	291	170	426	1.719	0.256
10	540	713	150	316	340	137	335	184	468	1.819	0.268
20	591	766	163	329	377	171	376	196	500	1.921	0.278
30	644	815	175	340	421	205	418	206	530	2.033	0.289
40	684	863	192	351	453	238	454	216	560	2.099	0.294
50	726	907	200	362	494	270	492	223	581	2.209	0.303
60	761	946	203	373	538	301	528	224	588	2.357	0.314
70	799	978	220	382	575	336	563	232	613	2.423	0.319
80	818	1005	213	391	625	371	597	223	594	2.682	0.334
90	845	1028	210	401	681	398	630	215	580	2.925	0.347
100	868	1047	216	409	717	436	662	213	578	3.102	0.354

TABLE III

Calculated elastic C_{ij} [GPa], bulk modulus B [GPa], shear modulus G [GPa], Young's modulus E [GPa], Poisson's ratio ν, and B/G ratio of HfN_2 under pressure [GPa].

P	C_{11}	C_{33}	C_{44}	C_{66}	C_{12}	C_{13}	B	G	E	B/G	ν
0	562	700	173	321	276	134	323	209	515	1.550	0.235
10	627	766	196	337	307	173	369	228	568	1.618	0.244
20	692	826	219	350	343	212	416	246	617	1.688	0.253
30	751	885	242	361	374	250	460	263	663	1.745	0.259
40	805	941	266	372	402	293	503	279	706	1.802	0.266
50	865	997	281	379	442	326	546	292	743	1.873	0.273
60	919	1051	300	393	478	362	588	305	781	1.927	0.279
70	967	1104	318	402	512	402	630	317	814	1.989	0.285
80	1016	1155	335	410	551	437	671	328	846	2.047	0.290
90	1063	1205	355	417	587	473	711	339	878	2.095	0.294
100	1108	1254	368	425	627	511	752	347	902	2.168	0.300

Poisson's ratio ν as given in Eq. (16) is used to evaluate the stability parameters of the shear resistance of materials [23]:

$$\nu = \frac{3B - 2G}{2(3B + G)}. \tag{16}$$

It could be noted that the higher the value of ν, the better the plasticity of material. It is shown that the value of ν increased with an increase in pressure (Tables II and III), which is consistent with the prediction of B/G.

For ZrN_2 and HfN_2, the elastic constants in the range from 0 GPa to 100 GPa are calculated. The elastic constants of ZrN_2 are plotted in Fig. 3a. It can be seen that the elastic constants C_{ij} monotonically grow with an increase in pressure P. The elastic constants of ZrN_2 are plotted in Fig. 3b and all the C_{ij} of HfN_2 increase linearly with an increase in pressure. For ZrN_2 and HfN_2, C_{11} and C_{33} increase much faster as compared to other elastic constants with an increase in pressure, which shows that the elastic constants of the two directions increase

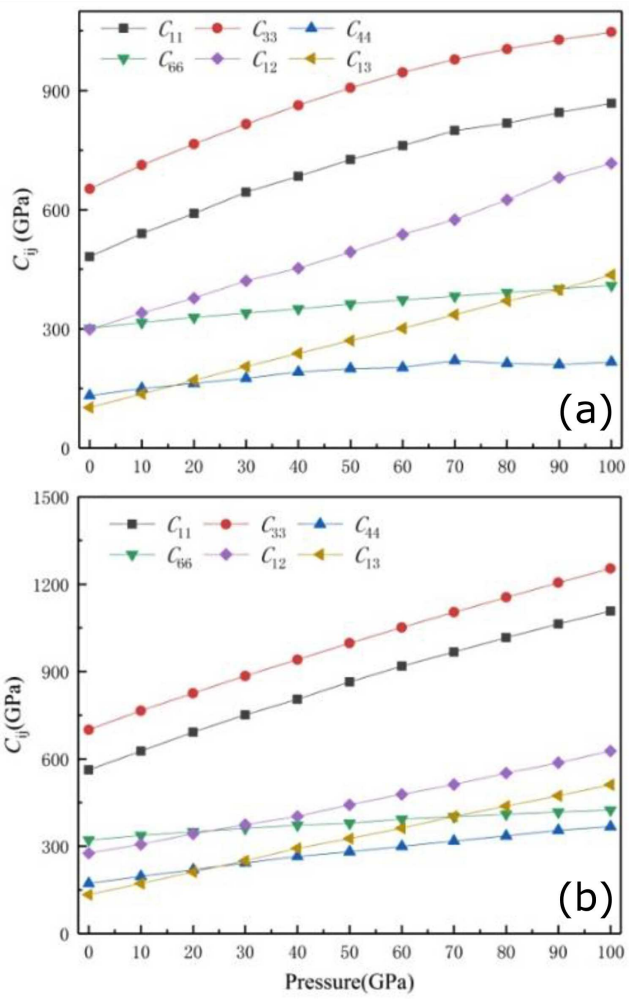

Fig. 3. (a) Pressure dependence of the elastic stiffness coefficients (C_{ij}) of ZrN_2 at 0 K. (b) Pressure dependence of the elastic stiffness coefficients (C_{ij}) of HfN_2 at 0 K.

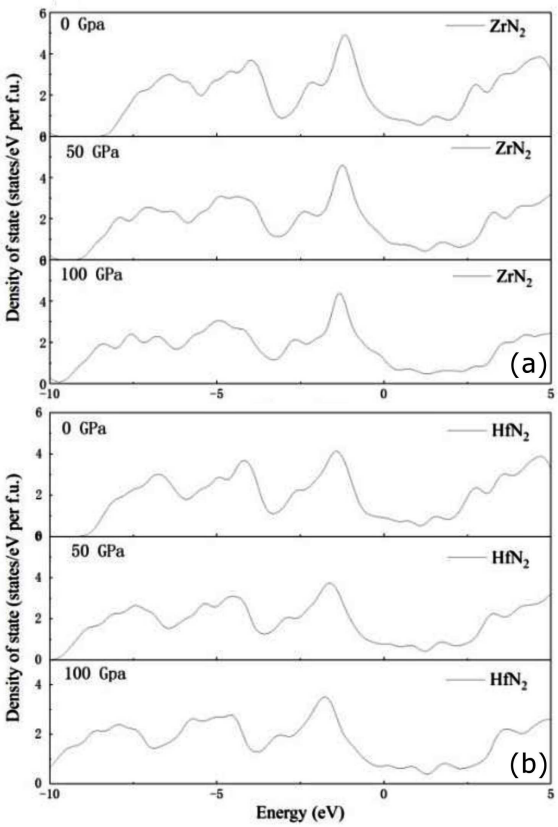

Fig. 4. (a) The density of states for ZrN_2 at 0, 50, and 100 GPa. (b) The density of states for HfN_2 at 0, 50, and 100 GPa.

more easily than the other by the effect of pressure elastic constants. For transition metals, C_{11} and C_{33} are very important, which are related to atomic bonding and deformation behavior. $C_{33} > C_{11}$, indicating that the atomic bond on the {100} shear plane is stronger than {001}, as shown in Fig. 3a and b.

The density of states (DOS) is a visual representation of the energy band structure, which is usually combined with the DOS to analyze the properties such as the crystal structure. However, since it is more visualized than the energy band graph, it is more widely used in the analysis. The DOS are calculated at 0, 50, and 100 GPa and the evolution of electrons was examined for ZrN_2 (Fig. 4a) and HfN_2 (Fig. 4b) under the above pressures. It can be seen that the DOS obtained at 0 GPa are consistent with the previous calculations and demonstrate similar contours under the above pressures. As shown in Fig. 4, both ZrN_2 and HfN_2 display metal properties under 0, 50, as well as at 100 GPa.

3.3. Elastic anisotropy

The anisotropy of crystals is different along the direction of lattice, and also the periodicity and density of the atoms are different, which leads to different physical and chemical properties of crystals in different directions [24]:

$$A_1 = \frac{4C_{44}}{C_{11} + C_{33} - 2C_{13}}, \quad (17)$$

$$A_2 = \frac{4C_{55}}{C_{22} + C_{33} - 2C_{23}}, \quad (18)$$

$$A_3 = \frac{4C_{66}}{C_{11} + C_{22} - 2C_{12}}. \quad (19)$$

A_1 represents the shear anisotropy factor of the {100} shear plane between ⟨011⟩ and ⟨010⟩; A_2 represents the shear anisotropy factor of the {010} shear plane between ⟨101⟩ and ⟨001⟩; A_3 represents the shear anisotropy factor of the {001} shear plane between ⟨110⟩ and ⟨010⟩. The A_1, A_2, and A_3 of the isotropic crystals must be equal to 1. If A_1, A_2, and A_3 of some of the crystals are not equal to 1, then the crystals are not anisotropic. A_1 and A_2 are equal as ZrN_2 and HfN_2 belong to the tetragonal system.

TABLE IV

Calculated universal elastic anisotropy index A^U, shear anisotropic factors A_1, A_2, and percentage of anisotropy in compressibility and shear A_B and A_G of ZrN_2.

P	A^U	A_1	A_2	A_B	A_G
0	−1.134	0.567	3.284	2×10^{-4}	−0.128
10	−1.184	0.612	3.157	2×10^{-4}	−0.134
20	−1.217	0.642	3.079	2×10^{-4}	−0.139
30	−1.222	0.668	3.046	3×10^{-4}	−0.139
40	−1.212	0.716	3.030	2×10^{-4}	−0.138
50	−1.165	0.732	3.114	2×10^{-4}	−0.132
60	−1.052	0.734	3.341	3×10^{-4}	−0.118
70	−0.992	0.796	3.401	4×10^{-4}	−0.110
80	−0.674	0.787	4.064	4×10^{-4}	−0.072
90	−0.257	0.781	4.880	9×10^{-4}	−0.027
100	0.016	0.829	5.407	9×10^{-4}	0.001

TABLE V

Calculated universal elastic anisotropy index A^U, shear anisotropic factors A_1, A_2, and percentage of anisotropy in compressibility and shear A_B and A_G of HfN_2.

P	A^U	A_1	A_2	A_B	A_G
0	0.512	0.695	2.244	3×10^{-6}	0.049
10	0.401	0.751	2.106	4×10^{-6}	0.039
20	0.323	0.801	2.001	8×10^{-7}	0.031
30	0.264	0.854	1.916	1×10^{-5}	0.026
40	0.217	0.915	1.849	8×10^{-5}	0.021
50	0.196	0.930	1.795	3×10^{-5}	0.019
60	0.187	0.963	1.784	3×10^{-5}	0.018
70	0.177	1.005	1.764	6×10^{-5}	0.017
80	0.178	1.035	1.762	5×10^{-5}	0.017
90	0.179	1.074	1.751	6×10^{-5}	0.018
100	0.189	1.098	1.766	6×10^{-5}	0.019

The anisotropic factor which varies with pressure in the structure of ZrN_2 and HfN_2 are shown in Tables IV and V, respectively. For ZrN_2, the shear anisotropic factors A_1 at 0 GPa is 0.567, and at 100 GPa is 0.829; whereas the shear anisotropic factors A_2 at 0 GPa is 3.284, and at 100 GPa is 5.407. In case of HfN_2, the shear anisotropic factors A_1 at 0 GPa is 0.695 and at 100 GPa is 1.098; whereas the shear anisotropic factors A_2 at 0 GPa is 2.244, and at 100 GPa is 1.766. It could be noted from the above tables that these two anisotropic factors are not equal to 1, which indicates that ZrN_2 and HfN_2 are also anisotropic. A_1 and A_2 increase with an increase in pressure and are far away from 1, as shown in Table IV. It is exhibited that the shear anisotropy of {100} ,{010}, and {001} of the shear planes increase with an increase in pressure for ZrN_2. A_1 increases with an increase in pressure and is far away from 1, while A_2 decreases with an increase in pressure, and then becomes close to 1 as indicated in Table V. It is also found that for HfN_2 the shear anisotropy of {100} and {010} of the shear planes increases with an increase in pressure, while the shear anisotropy of {001} of the shear planes decrease with an increase in pressure.

B_V and G_V can be obtained from the elastic constants C_{ij} as follows [23]:

$$B_V = \frac{1}{9}[C_{11} + C_{22} + C_{33} + 2(C_{12} + C_{13} + C_{23})], \quad (20)$$

$$G_V = \frac{1}{15}[C_{11} + C_{22} + C_{33} + 3(C_{44} + C_{55} + C_{66}) - (C_{12} + C_{13} + C_{23})]. \quad (21)$$

We can obtain the B_R and G_R from the elastic constants C_{ij} [23]:

$$B_R = \Delta[C_{11}(C_{22} + C_{33} - 2C_{23}) + C_{22}(C_{33} - 2C_{13}) - 2C_{33}C_{12} + C_{12}(2C_{23} - C_{12}) + C_{13}(2C_{12} - C_{13}) + C_{23}(2C_{13} - C_{23})]^{-1}, \quad (22)$$

$$G_R = 15\left\{4[C_{11}(C_{22} + C_{33} + C_{23}) + C_{22}(C_{33} + C_{13}) + C_{33}C_{12} - C_{12}(C_{23} + C_{12}) - C_{13}(C_{12} + C_{13}) - C_{23}(C_{13} + C_{23})]/\Delta + 3\left(\frac{1}{C_{44}} + \frac{1}{C_{55}} + \frac{1}{C_{66}}\right)\right\}^{-1}, \quad (23)$$

where

$$\Delta = C_{13}(C_{12}C_{23} - C_{13}C_{22}) + C_{23}(C_{12}C_{13} - C_{23}C_{11}) + C_{33}(C_{11}C_{22} - C_{12}^2). \quad (24)$$

The universal elastic anisotropy index A^U is obtained by the following equation [25]:

$$A^U = 5\frac{G_V}{G_R} + \frac{B_V}{B_R} - 6. \quad (25)$$

When A^U is 0, it is shown that the solid is isotropic or anisotropic. For ZrN_2, the elastic anisotropy index at 0 GPa is −1.134, which suggests that it is anisotropic. When the pressure increases from 0 GPa to 100 GPa, the value of A^U for ZrN_2 increases from −1.134 to 0.016, whereas for HfN_2, the elastic anisotropy index at 0 GPa is 0.512, which suggests that it is anisotropic. When the

pressure increases from 0 GPa to 100 GPa, the value of A^U for HfN_2 decreases from 0.512 to 0.189. Moreover, all of them are not equal to 0, which indicates an elastic anisotropy.

The percentage anisotropy in compressibility and shear are defined as follows [25]:

$$A_B = \frac{B_V - B_R}{B_V + B_R}, \tag{26}$$

$$A_G = \frac{G_V - G_R}{G_V + G_R}. \tag{27}$$

The values of isotropic crystal are 0 and the values of A_B and A_G suggest that the structures of ZrN_2 and HfN_2 are anisotropic in compressibility and shear.

TABLE VI

Young's modulus maximum $E_{\max}$ [GPa], minimum $E_{\min}$ [GPa] and average value E_{avg} [GPa] for ZrN_2 and HfN_2 in 0 GPa and 100 GPa.

	ZrN_2		HfN_2	
E	0 GPa	100 GPa	0 GPa	100 GPa
$E_{\max}$	667.556	979.956	707.021	1033.65
$E_{\min}$	292.860	268.784	410.969	704.866
E_{avg}	437.288	596.361	527.466	912.781

The descriptions on the three-dimensional surface of Young's modulus E for ZrN_2 and HfN_2 at 0 GPa and 100 GPa are shown in Fig. 5a and c and Fig. 6a and c, respectively. For isotropic crystals, the three-dimensional surface description should be spherical. A divergence from the spherical shape can reflect the level of elastic anisotropy. It is obvious that they are not spherical

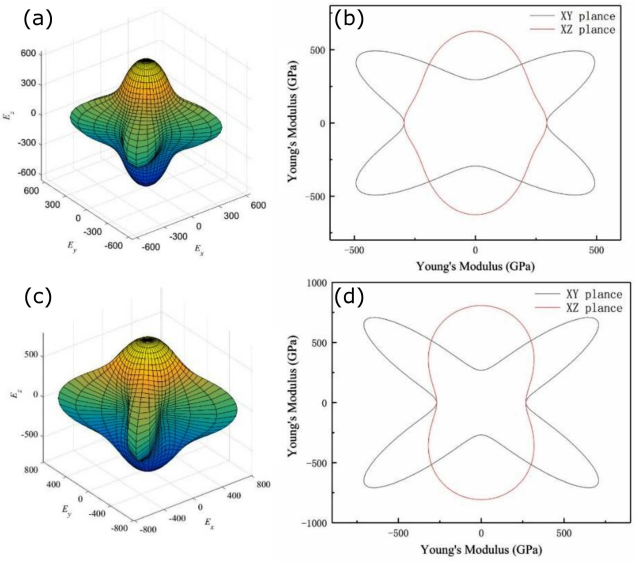

Fig. 5. (a) Direction dependence of three-dimensional surface description (b) and plane projection on Young's modulus for ZrN_2 in 0 GPa. (c) Direction dependence of three-dimensional surface description (d) and plane projection on Young's modulus for ZrN_2 in 100 GPa.

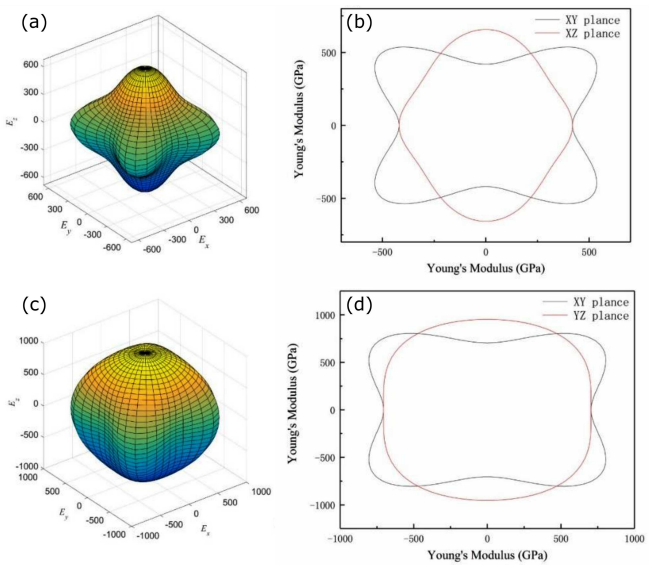

Fig. 6. (a) Direction dependence of three-dimensional surface description (b) and plane projection on Young's modulus for HfN_2 in 0 GPa. (c) Direction dependence of three-dimensional surface description (d) and plane projection on Young's modulus for HfN_2 in 100 GPa.

in Figs. 5 and 6. It could be concluded that ZrN_2 and HfN_2 have obvious anisotropy. Furthermore, the projections of three-dimensional surface depictions of Young's modulus E for ZrN_2 and HfN_2 at 0 GPa and 100 GPa are displayed in Fig. 5b and d and Fig. 6b and d, respectively. Young's modulus maximum E_{max} (GPa), minimum E_{min} (GPa), and average value E_{avg} (GPa) for ZrN_2 and HfN_2 at 0 GPa and 100 GPa are indicated in Table VI. For ZrN_2, the average value of Young's modulus at 0 GPa is 667.556 and at 100 GPa it is 596.361. For HfN_2, the average value of Young's modulus at 0 GPa is 527.466 and at 100 GPa is 912.781. It could be noted that E_{min} is in the XZ plane for ZrN_2 at 0 GPa and 100 GPa, and E_{min} is in the XY plane for HfN_2 at 0 GPa and 100 GPa. It is obvious that ZrN_2 and HfN_2 have a plane anisotropy expression in all the planes.

4. Conclusions

The crystal structure, elastic constants, and anisotropy parameters of ZrN_2 and HfN_2 are calculated by first-principle calculations. The observed results are listed as follows: (1) As the pressure increases, the ratio of the volume of primitive cell is observed to change from 1 to 0.804 for ZrN_2, which is more easily compressed along c-axis of the crystal than a-axis. As pressure increases, the ratio of the volume of primitive cell changes from 1 to 0.823 for HfN_2, which is more easily compressed along a-axis of the crystal than c-axis. (2) The structures of ZrN_2 and HfN_2 are stable from 0 GPa to 100 GPa. (3) For ZrN_2, the bulk modulus and the shear modulus are 291 GPa and 170 GPa, respectively, at 0 GPa, whereas the bulk modulus and the shear modulus for HfN_2 are 323 GPa and 209 GPa, respectively, at 0 GPa. The bulk

modulus and shear modulus increase with an increase in pressure. (4) The obtained B/G ratio indicates that ZrN_2 and HfN_2 possess ductility in the studied pressure ranges. (5) ZrN_2 and HfN_2 show anisotropy at 0 and at high pressure.

Acknowledgments

This work is supported by the National Natural Science Foundation of China (Grant No. 61474089), and the Natural Science Foundation from Education Committee of Shaanxi Province, China (Grant No. 16JK1016).

References

[1] X. Yan, M. Chi, P.D. Han, B.S. Xu, *J. Taiyuan Univ. Technol.* **39**, 23 (2008).

[2] F. Colmenares, S. Melendez, *Chem. Phys. Lett.* **380**, 292 (2003).

[3] R. Yu, Q. Zhan, L.C.D. Jonghe, *Angew. Chem. Int. Ed.* **46**, 1136 (2007).

[4] R. Yu, Q. Zhan, X.F. Zhang, *Appl. Phys. Lett.* **86**, 051913 (2006).

[5] R. Yu, X.F. Zhang, *Phys. Rev. B* **72**, 054103 (2005).

[6] R. Yu, X.F. Zhang, *Appl. Phys. Lett.* **86**, 121913 (2005).

[7] A. Erdemir, *Tribol. Int.* **38**, 249 (2005).

[8] J.C. Crowhurst, A.F. Goncharov, B. Sadigh, C.L. Evans, P.G. Morrall, J.L. Ferreira, A.J. Nelson, *Science* **311**, 1275 (2006).

[9] E. Gregoryanz, C. Sanloup, M. Somayazulu, J. Badro, G. Fiquet, H.-K. Mao, R.J. Hemley, *Nature Mater.* **3**, 294 (2004).

[10] J.A. Montoya, A.D. Hernandez, C. Sanloup, E. Gregoryanz, S. Scandolo, *Appl. Phys. Lett.* **90**, 011909 (2007).

[11] A. Yildiz, U. Akinci, O. Gülseren, I. Sökmen, *Inst. Phys. J.* **21**, 485 (2009).

[12] A. Young, J. Montoya, C. Sanloup, M. Lazzeri, E. Gregoryanz, S. Scandolo, *Phys. Rev. B* **73**, 2 (2006).

[13] G. Soto, *Comput. Mater. Sci.* **61**, 1 (2012).

[14] P. Hohenberg, W. Kohn, *Phys. Rev.* **136**, B1864 (1964).

[15] W. Kohn, L.J. Sham, *Phys. Rev.* **140**, A1133 (1965).

[16] S.J. Clark, M.D. Segall, C.J. Pickard, P.J. Hasnip, M.I.J. Probert, K. Refson, M.C. Payne, *Z. Kristallogr.* **220**, 567 (2005).

[17] D.M. Ceperley, B.J. Alder, *Phys. Rev. Lett.* **45**, 1566 (1980).

[18] J.P. Perdew, A. Zunger, *Phys. Rev. B* **23**, 5048 (1981).

[19] M.G. Zhang, K. Cheng, H.Y. Yan, Q. Wei, B.B. Zheng, *Sci. Rep.* **6**, 36911 (2016).

[20] S.H. Zhang, R.F. Zhang, *Comput. Phys. Commun.* **220**, 403 (2017).

[21] R. Hill, *Proc. Phys. Soc. Sect. A* **65**, 349 (1952).

[22] G.V. Sin'ko, N.A. Smirnov, *J. Phys. Condens. Matter* **14**, 6989 (2002).

[23] S.F. Pugh, *Philos. Mag.* **45**, 823 (1954).

[24] Q. Zhang, Q. Wei, H.Y. Yan, Q.Y. Fan, X.M. Zhu, J.Q. Zhang, D.Y. Zhang, *Z. Naturforsch. A* **71**, 387 (2016).

[25] M.J. Xing, X.Z. Li, S.J. Yu, F.Y. Wang, *Commun. Theor. Phys.* **68**, 395 (2017).

[26] Q.Y. Fan, Q. Wei, C.C. Chai, Y.T. Yang, X.H. Yu, L. Yang, J.P. Zheng, P.K. Zhou, D.Y. Zhang, *Acta Phys. Pol. A* **129**, 103 (2016).